

# Project Report

Group 14: Joanna Broniarek (1868264), Ivana Nastasic (1852026)

## Brain network study during resting states Bioinformatics - Project I

November 25, 2019



## Contents

Introduction	2
Data	2
1 Connectivity graphs	2
2 Graph theory indices	3
3 Motif analysis	4
4 Community detection	5
5 Conclusions	5
Methods	6
Tables	6
Images	9

# Introduction

Goal of this project is to analyze two data sets of EEG data and to make a comparison between them. An electroencephalogram (EEG) is a test that detects electrical activity in brain using electrodes attached to a scalp. Detailed list of performed tasks is given in the **Table 1**.

## Data

The EEG data are available from PhysioNet, “EEG Motor Movement/Imagery Dataset” [1]. They are recorded from 64 electrodes with subject at rest in eyes-open and eyes-closed conditions, respectively. For our work we used only data from subject identified as "S086" collected in the first 2 runs: R01 is recorded during eyes-open (EO) and R02 is recorded during eyes-closed (EC) resting states.

## 1 Connectivity graphs

Brain connectivity estimators represent patterns of links in the brain [3]. There are several methods for estimation of functional connectivity from multichannel data. Two widely used methods are Directed Transfer Function (DTF) and Partial Directed Coherence (PDC), statistical techniques based on autoregressive modeling of multivariate time series (MVAR) in conjunction with the concept of Granger Causality provide clues to directional connectivity and magnitude of information flow between neuronal ensembles.

### Task 1.1 & 1.2

We estimated functional brain connectivity among 64 channels using both PDC and DTF estimators. Akaike information criterion (AIC) is used to determine the proper model order  $p$  for our study. Graph 1 illustrates the obtained relationship between different model order  $p$  and estimation error  $E(t)$ . According to these results the best AIC order is equal to 7. For the resolution of the model we chose 100 and for frequency value we chose 10 Hz, since we are dealing with the waves recorded from the brain in resting state which corresponds to Alpha waves whose frequency is within the range 8-12 Hz.

Then, we applied an appropriate threshold for results of both estimators in order to get the binary adjacency matrices with network densities approximately 20%. The Figures 2 and 3 show graphically represented the binary adjacency matrices in both resting states for PDC and DTF methods respectively. After the analysis of these figures, we did not find any significant differences between Eyes-Open and Eyes-Closed resting states for each estimator. In the case of PDC the highest connectivity seems to be in the middle and the bottom-right parts of matrices. In the case of DTF the highest connectivity prone to be in the right parts. The matrix for Eyes-Open state seems to have slightly more connections in the middle part. However, taking into account comparison between PDC and DTF method, it is visible that they are focused on different connections between channels. Indeed, PDC shows only direct flows between channels. Unlike DTF, PDC is normalized to show a ratio between the outflow from channel  $j$  to channel  $i$  to all the outflows from the source channel  $j$ , so it emphasizes rather the sinks, not the sources [5].

### Task 1.3

As the next step, we performed an analysis of results from PDC and DTF estimators for seven different network densities: 1%, 2%, 5%, 10%, 20%, 30% and 50%. The corresponding plots can be found at Figure 4. As previously, in the PDC case, we did not identify any significant difference between resting states for each density. However, it is noticeable that for increasing percentage of density, the matrices are getting more dense in the bottom parts. Additionally, for some channels in EO, the increased density results with increased number of connections but only in the same direction (out/in). The channels with this behaviour are slightly different comparing EO and EC states. In the case of DTF, matrices for each density and each condition seems to be very similar. Moreover, the higher density, the more one-directional connections to channels in the right part of matrix.

### Task 1.4

This time, we considered the subset of 19 channels and estimated the connectivity using PDC method, applying a statistical validation method which is resampling/bootstrap procedure with 200 replications. As the result of this procedure, we obtained filtered out values that are not significantly different from 0 with significance level 5%. The corresponding graphical representations of matrices with densities 20% for both resting states are shown in Figure 5. In the state of Eyes-Open the connections are mostly located in the center part of matrix, whereas in the state of Eyes-Closed we also can notice more connections in the middle part and additionally more edges with channel 3 (F7), but only in one direction.

### Task 1.5

In order to visualise the connections of channels with respect to the real topology, we made a topographical representation of them with the coordinates provided in the file channel\_locations.txt. The following types of networks for both resting states are presented: A) in the Figure 6 the 64-channel, PDC networks with densities 5%; B) in the Figure 7 the 64-channel, DTF networks with densities 5%. In the case of PDC (A) the networks are more dense in the Parietal and Frontal part of scalp in both rest conditions. There also is a channel P1 that has many outgoing edges. However, in the case of DTF (B), networks look different in comparison to PDC ones. Two channel in Parietal Part (P3, Po3) have many incoming edges in both resting states. The network in EO condition seems to have few more connections in the upper part of network than in EC condition.

### Task 1.6

In addition to above analysis, we performed connectivity estimation with the use of PDC method with another **frequency 20 Hz**, which belongs to the range of Beta waves. The Figure 8 presents the graphical representation of the binary adjacency matrix with density 20%, obtained in this task. We could expect that when the patient opens his eyes, the beta waves replace alpha waves and the difference between states would be noticeable [6]. However, there is no difference between Eyes-Open and Eyes-Closed states.

## 2 Graph theory indices

### Task 2.1 & 2.3 & 2.6

#### GLOBAL INDICES:

- a) **Clustering coefficient** is a measure of the degree to which nodes in a graph tend to cluster together, with values in range 0 to 1. Formula for node  $n$  is:  $C_n = e_n/(k_n(k_n - 1))$ , where  $e_n$  is the number of connected pairs between all neighbors of node  $n$  and  $k_n$  is the number of neighbors.
- b) **Average shortest path length** is the average path length evaluated among all the shortest path computed for a graph.

#### LOCAL INDICES:

- a) **Degree** of a node is the number of edges connected to the node.
- b) **In-degree** is the number of incoming edges into a node.
- c) **The out-degree** is the number of outgoing edges emanating from a node.

We analyzed properties of graphs created in Task 1.1. (10Hz) and 1.6.(20Hz). Global indices for EO and EC states, calculated from PDC estimation on 10Hz and 20Hz can be found in Table 2 and Table 4, respectively. In both cases, there is no significant difference between EO and EC state in terms of clustering coefficient. There is a small difference in avg shortest path length between two states. We computed local measures state and selected the first 10 nodes with highest degrees. The results for PDC (10Hz) are in Table 5 and 6. We notices, that the nodes with the highest degree mainly come from the parietal area in both EC and EO.

The values of the global indices for EO and EC states based on DTF estimation (10Hz) can

be found in Table 3. Comparing this result with one obtained from PDC estimation, we noticed that graph generated from DTF led to smaller average shorter path length and to higher clustering coefficient. However, the local indices values doesn't show significant difference for EO and EC state.

### Task 2.2

A **small-world network** is a type of mathematical graph in which most nodes can be reached from every other node by a small number of steps. Specifically, a small-world network is defined to be a network where the typical distance  $L$  between two randomly chosen nodes grows proportionally to the logarithm of the number of nodes  $N$  in the network, that is:  $L \propto \log N$  [9].

A graph  $G$  with  $n$  nodes and  $m$  edges is a small-world network, if it has a similar path length but greater clustering of nodes than an equivalent Erdős-Rényi (E–R) random graph, with the same  $m$  and  $n$  (an E–R graph is constructed by uniquely assigning each edge to a node pair with uniform probability). The formula for small-coefficient is  $\sigma = \frac{C_G}{C_{ER}} \frac{L_{ER}}{L_G}$ , where  $C_G$ ,  $C_{ER}$  are average clustering coefficients of graph  $G$  and its' equivalent E–R graph and  $L_G$  and  $L_{ER}$  are average shortest path lengths of graph  $G$  and its' E–R graph. If  $\sigma$  is greater than 1, graph  $G$  can be considered a small-world network. [10] The calculated  $\sigma$  values for EO and EC are 1.65 and 1.28, respectively, thus both networks could be considered as small-world.

### Task 2.4

We compared global indices considering the same different network densities as Task 1.3. As we can see from the Figure 9, while the network density increases, the clustering coefficients grow similarly in both rest states. Moreover, the average shortest path length is the highest in case of the network density of 20% for both EO and EC case.

## 3 Motif analysis

**Network motifs** are statistically overrepresented sub-graphs in a network, and have been recognized as ‘the simple building blocks of complex networks’. Stating that they are statistically overrepresented means that their frequency is significantly higher than what would be expected in similar random networks [11]. However, **antimotifs** are significantly underrepresented subnetworks.

### Task 3.1

For motif analysis we decided to set up the following parameters as an input to the program:  $s = 3$ , which corresponds to size of a motif to be detected and  $r = 1000$  as a number of generated random networks. Figure 10 shows a comparison between frequency spectrum of 3-node motifs for both resting states. The differences between two conditions are not sufficiently great. However, for majority of motifs the EC state network contains few more such configurations. Interesting is that motif 36 is the most common motif in both conditions.

Table 7 and Table 8 contain the summaries of the statistics from program. Both rest-states obtained similar motifs, apart from the motif 108 in the EC state. This motif represents the configuration coded as [001 101 100]. Such a difference in comparison to EO state can be result of slightly more dense network in the EC state.

### Task 3.2

We performed more detailed analysis of the motif with pattern  $A \rightarrow B \leftarrow C$ , which corresponds to motif id 36. We created a topographical representation of the networks considering only the connections involved in this configuration. Figure 11 presents obtained networks. The connections are very dense in Parietal, Central and Frontal regions for both conditions. However, in the EC state the central part is even more connected.

### Task 3.3

As a next step, we selected one channel in parieto-occipital scalp region (**channel POz**) and determined all motifs related to it. Figure 13 shows the edges of all motifs where the selected channel was involved. Comparing two resting conditions, we can notice many differences. In the Eyes-Open state the channel Poz has just few connections with the nearest channels (mostly in Parietal part). On the other hand, in the Eyes-Closed state the same channel has many more edges incoming from

Frontal region. Another very interesting channel is Po3 in Parieto-Occipital scalp, with even more incoming connections than Poz. This means that parieto-occipital region has a huge significance in terms of distinguishing two rest-states and is more active for alfa waves in Eyes-Closed state.

#### Task 3.4

We replied the analysis of the same graph but this time considering 4-node motifs. Because of the limited space, we did not located the Table in this report, but as an external file. In the case of Eyes-Open state we obtained less motifs (30) than in the Eyes-Closed state (32). However, majority of them is the same.

## 4 Community detection

Communities or clusters are usually groups of nodes having higher probability of being connected to each other than to members of other groups. Identifying communities is an ill-defined problem. There are no universal rules, like the definition of community itself, nor other crucial issues, like the validation of algorithms and the comparison of their performances [12].

One common approach to detect communities is modularity maximization, in which one seeks a partition of a network that maximizes *modularity* - an objective function that quantifies the extent to which nodes in a community connect with one another in comparison to some baseline [13].

Another approach to analyze community network is based on the theory of information flow. It aims to identify communities by optimally compressing a description of information flows on the network. The nodes among which information flows quickly and easily are clustered as a well-connected community [14].

#### Task 4.1 & 4.2 & 4.3

In order to detect and compare communities in our graphs we applied two algorithms that comes from the described approaches. The first one is **Louvain modularity-based algorithm** [15]. We applied this method for the networks from the first part of report that are estimated by PDC and DTF methods with density 10% for both Eyes-Open and Eyes-Closed conditions. We also made a graphical representation of these community structures. They are presented in the Figure 14 and Figure 15, respectively.

In case of PDC and DTF networks and Louvain algorithm, the number of detected communities is the same for both rest-states. However, the members of these clusters are different (see Table 9 and 10). More specifically, the frontal part of a scalp is divided into two clusters in EC, rather than one cluster as it is in EO. The same community-splitting behaviour presents the parieto-occipital part. As Louvain algorithm is based on modularity it can suggests that dependently on the rest state there are regions of more/less dense edges.

The second method that we used is **Infomap** algorithm, which is based on **the principles of information theory**. The algorithm maximizes an objective function called the Minimum Description Length. The basic idea behind the InfoMap algorithm is to use community partitions of the graph as a Huffman code that compresses the information about a random walker exploring the graph [16]. The graphical representation of the results can be found in the Figure 16 and 17.

In the case of Infomap algorithm and PDC networks, differences between states are not so big as previously. However, we obtained an interesting result for DTF networks, where for the Eyes-Open state the clusters are scattered in many places, whereas for Eyes-Closed there is a big cluster containing channels mostly from Parieto-Occipital region and Frontal region. This suggests that there is a higher information flow throught nodes of this cluster. Lists of nodes can be found in Table 11 and 12.

## 5 Conclusions

The connectivity analysis from part 1, showed that estimation methods PDC and DTF are focused on different connections between channels. Nevertheless, both of them highlight the Parietal part of

scalp as important for nodes communication in resting states. This is also confirmed in the graph indices analysis where those nodes appear in majority of nodes with the highest degree.

Through the motif analysis we found out that there are few channels in parieto-occipital region that perform very high communication with frontal region during Eyes-Closed state, what does not occur in Eyes-Open state. Because the connections to these channels are mostly in-coming, this also explains why the motif with pattern  $A \rightarrow B \leftarrow C$  is the most frequent one in networks.

However, the Community Detection part let us understand how dissimilar approaches can differently estimate community structures. In particular, the Infomap algorithm confirmed that information flow is not the same in both resting states and that the alpha waves are changing for specific parts of scalp.

We believe the overall results described in this report are helpful in understanding communication in brain networks and enables to highlight the functional associations among brain regions, as well.

## Methods

We applied Python library **pyedflib** to load data [2] and **numpy** module for general data pre-processing. In order to fit MVAR models and estimates connectivity with TDF and PDC methods, we used the Python module **ConnectivityPy**[5]. Motif Analysis was performed with the use of open-source tool **mFinder** [8]. For the part of Community Detection we used the python modules: **igraph**, **louvain**, **infomap**. However, for the whole networks and matrices visualisation we took advantage of few graphical Python libraries: **networkx**, **matplotlib** and **seaborn**.

## Tables

Task	1.1	1.2	1.3	1.4	1.5	2.1	2.2	2.3	2.4	2.6
Class	mandatory	A	A	D	C	mandatory	D	B	C	B
Task	3.1	3.2	3.3	3.4	4.1	4.2	4.3			
Class	mandatory	C	C	E	mandatory	B	C			

Table 1: Lists of tasks chosen in the project

	Clustering coefficient	Avg shortest path length
EO	0.39	2.27
EC	0.35	2.52

Table 2: Global indices PDC 10Hz

	Clustering coefficient	Avg shortest path length
EO	0.64	1.81
EC	0.64	1.64

Table 3: Global indices DTF 10Hz

	Clustering coefficient	Avg shortest path length
EO	0.39	2.94
EC	0.4	2.7

Table 4: Global indices PDC 20Hz

Degree		In-degree		Out-degree	
Channel	Degree	Channel	Degree	Channel	Degree
Fp2	58	P4	34	P1	49
Fpz	50	Fz	34	Af8	43
P1	49	Po3	33	Fp2	37
P4	48	P3'	29	Fpz	37
Af8	46	Po4	26	C5	30
Fz	43	F2	25	T8	29
Po3	41	P6	23	T9	26
P6	39	Cpz	22	Af4	26
Po4	37	Fp2	21	Af7	26
P3	35	Cp2	21	F6	25

Table 5: Local indices PDC 10Hz, Eyes-Open

Degree		In-degree		Out-degree	
Channel	Degree	Channel	Degree	Channel	Degree
Po3	48	Po3	35	P1	48
P1	48	P3	32	Af8	37
P4	43	P4	29	Af7	33
P3	40	P2	26	Fpz	31
Po8	39	Fp1	26	Fp2	30
Fp2	39	Po8	24	F6	25
P2	38	Poz	24	F8	24
Af8	38	Pz	24	Af4	23
Fpz	38	Oz	21	F7	21
Poz	37	Fc4	21	T7	20

Table 6: Local indices PDC 10Hz, Eyes-Closed

Motif ID	$f_G(G_k)$	$f_{\hat{G}}(G_k)$	Z-score	$P(f_G(G_k) > f_{\hat{G}}(G_k))$	$f'_G(G_k)$	(Anti)motif
<b>6</b>	4101	4161.6+-31.3	-1.94	0.980	15	None
<b>12</b>	1724	1621.6+-28.7	3.57	0.000	14	Motif
<b>14</b>	687	897.6+-26.1	-8.08	1.000	11	Antimotif
<b>36</b>	2679	2848.5+-30.0	-5.64	1.000	19	Antimotif
<b>38</b>	1786	1744.0+-26.1	1.61	0.053	14	None
<b>46</b>	338	210.5+-15.5	8.22	0.000	8	Motif
<b>74</b>	913	905.9+-26.7	0.27	0.404	10	None
<b>78</b>	106	174.8+-10.4	-6.60	1.000	8	Antimotif
<b>98</b>	16	38.9+-7.1	-3.23	1.000	5	Antimotif
<b>102</b>	95	170.8+-17.5	-4.32	1.000	7	Antimotif
<b>108</b>	349	330.4+-16.0	1.16	0.131	10	None
<b>110</b>	172	140.5+-9.3	3.38	0.001	8	Motif
<b>238</b>	27	14.6+-3.1	4.00	0.001	4	Motif

Table 7: Eyes-Open & 3-size motifs

Motif ID	$f_G(G_k)$	$f_{\hat{G}}(G_k)$	Z-score	$P(f_G(G_k) > f_{\hat{G}}(G_k))$	$f'_G(G_k)$	(Anti)motif
6	3621	3722.0+-31.2	-3.23	1.000	17	Antimotif
12	2223	2162.2+-32.9	1.85	0.037	17	None
14	454	688.3+-22.8	-10.30	1.000	10	Antimotif
36	2789	2985.6+-31.1	-6.33	1.000	18	Antimotif
38	1938	1881.0+-28.7	1.99	0.018	17	None
46	269	129.4+-12.5	11.16	0.000	10	Motif
74	885	9284.1+-24.7	-1.74	0.964	11	None
78	52	135.4+-8.9	-9.37	1.000	6	Antimotif
98	58	74.8+-10.5	-1.59	0.959	5	None
102	84	151.5+-14.3	-4.72	1.000	7	Antimotif
108	347	303.1+-14.1	3.12	0.000	11	Motif
110	118	95.4+-8.0	2.81	0.004	9	Motif
238	31	10.7+-2.7	7.46	0.000	6	Motif

Table 8: Eyes-Closed & 3-size motifs

	Open-Eyes																
1.	Fc5	Fc3	Fc1	Fcz	Fc2	Fc6	C1	Cz	Cp2	Fpz	Fp2	Af7	Af3	Afz	Af4	Af8	F3
	F1	F2	F4	F8	Ft7												
2.	Cpz	Cp4	Fz	Tp7	P5	P3	Pz	P2	P4	P8	Po3	Poz	Po4	Po8	Oz	O2	Iz
3.	C2	C4	C6	Cp5	Cp3	Cp1	Cp6	Fp1	F7	F6	Ft8	T8	T9	T10	Tp8	P1	P6
4.	Fc4	C5	C3	F5	T7	P7	Po7	O1									
	Closed-Eyes																
1.	Fcz	Fc6	C1	Cz	Cp1	Cp2	Fpz	Fp2	Af7	Af3	Afz	Af4	Af8	F1	Fz	F2	F4
	F6	F8	Ft8	T8	T10												
2.	Cp3	Fp1	F5	P7	P5	P3	P1	Po7	Po3	Poz	O1	Oz	Iz				
3.	C6	Cpz	Cp4	Cp6	Tp8	Pz	P2	P4	P6	P8	Po4	Po8	O2				
4.	Fc5	Fc3	Fc1	C5	C3	C2	F7	F3	Ft7								
	Fc2	Fc4	C4	Cp5	T7	T9	Tp7										

Table 9: Table of clusters and their nodes for **Louvain** algorithm & **PDC** & density 10%

	Open-Eyes															
1.	Cz	C4	C6	Cp3	Cpz	Cp2	Cp4	Cp6	Fp1	F5	Tp8	P7	P5			
	P3	Pz	P4	P6	P8	Po7	Po3	Poz	Po4	Po8	O1	O2	Iz			
2.	Fc3	Fcz	Fc2	Fc6	C5	C2	Cp5	Fpz	Fp2	Af7	Af3	Afz	Af4			
	Af8	F7	F1	Fz	F2	F4	F6	F8	Ft7	P2						
3.	Fc5	Fc1	Fc4	C3	C1	F3	T8	Tp7	P1	Oz						
4.	Cp1	Ft8	T7	T9	T10											
	Closed-Eyes															
1.	Fc5	Fc3	Fc2	C5	C3	Cp5	Cp3	Fp1	Af7	Af3	F7	F5	F3			
	F1	Ft7	T7	T9	Tp7	P7	P5	P3	P1	Po7	Po3					
2.	Fc6	Cz	C2	C4	C6	Cpz	Cp2	Cp4	Cp6	Af4	F2	F4	Ft8			
	Tp8	P2	P4	P6												
3.	Fc4	C1	T8	T10	Pz	P8	Poz	Po4	Po8	O1	Oz	O2	Iz			
4.	Fc1	Fcz	Cp1	Fpz	Fp2	Afz	Af8	Fz	F6	F8						

Table 10: Table of clusters and their nodes for **Louvain** algorithm & **DTF** & density 10%

Open-Eyes																		
1.	Fc5	Fc1	Fcz	Fc2	Fc4	Fc6	C5	C1	Cz	C2	C4	C6	Cp5	Cp3	Cp1	Cp6	Fp1	
	Fpz	Fp2	Af7	Af3	Afz	Af4	Af8	F7	F1	F2	F6	F8	Ft8	T7	T8	T9	T10	
	Tp7	Tp8	P5	P1	P6	O1	Oz	Cp2	F4	P2								
2.	Fc3	F3	C3															
3.	Cpz	Cp4	Fz	P3	Pz	P4	P8	Po3	Poz	Po4	Po8	O2	Iz					
4.	F5	Ft7	P7	Po7														
Closed-Eyes																		
1.	Fc5	Fc3	Fc1	C3	F7	F3	Ft7	Fcz	Fc6	C5	C1	Cz	C2	Cpz	Fpz	Fp2	Af7	
	Af3	Afz	Af4	Af8	F5	F1	F6	F8	Ft8	P1	T7	T9	Tp7					
2.	Fc2	Fc4	C4	Cp1	Fz	F2	F4											
3.	C6																	
4.	Cp5																	
5.	Cp3	Cp2	Cp4	Cp6	Fp1	Tp8	P7	P5	P3	Pz	P2	P4	P6	P8	Po7	Po3	Poz	
	Po4	Po8	O1	Oz	O2	Iz												

Table 11: Table of clusters and their nodes for **Infomap** algorithm & **PDC** & **density 10%**

Open-Eyes																		
1.	Fc5	Tp7	P1	Oz														
2.	Fc3	Fc1	Fcz	Fc2	Fc4	Fc6	C5	Cp5	Fpz	Fp2	Af7	Af3	Afz	Af4	Af8	F7	F1	Fz
	F2	F4	F6	F8	Ft7	P2												
3.	C3	C6	Cp1	Cp2	F3	Ft8	T8	T10	Tp8	P6	Po8	O2						
4.	C1																	
Closed-Eyes																		
1.	Fc5	Fc3	Af7	F3	C3	F7	F5	Ft7	T9									
2.	Fc1	Fc2	Fc4	C5	Cz	C2	Cp5	Cp3	Cpz	Cp2	Fp1	Af3	Afz	Af4	F1	Fz	F2	F4
	T7	Tp7	P7	P5	P3	Pz	P2	P4	P8	Po7	Po3	Poz	Po4	Po8	O1	Oz	O2	Iz
3.	Fcz	Cp1	Fpz	Fp2	Af8	F6	F8	P1										
4.	Fc6	C4	C6	Cp4	Cp6	Ft8	T8	Tp8	P6									

Table 12: Table of clusters and their nodes for **Infomap** algorithm & **DTF** & **density 10%**

## Images

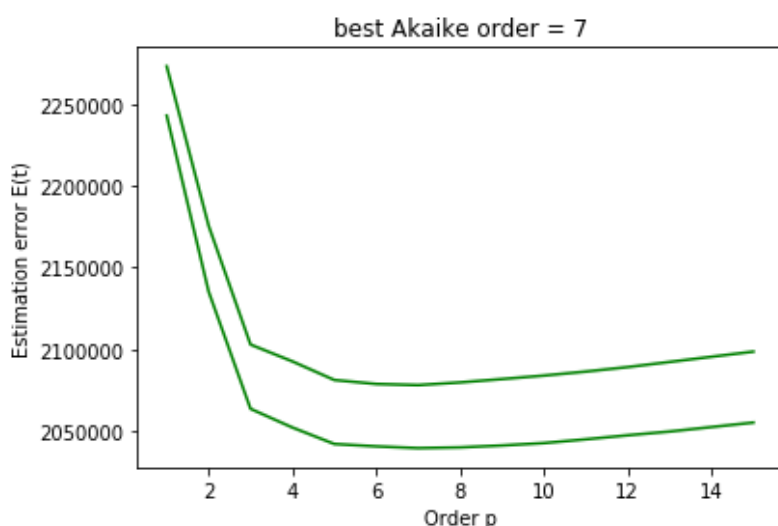


Figure 1: Akaike order vs. Estimation Error (Task 1.1).

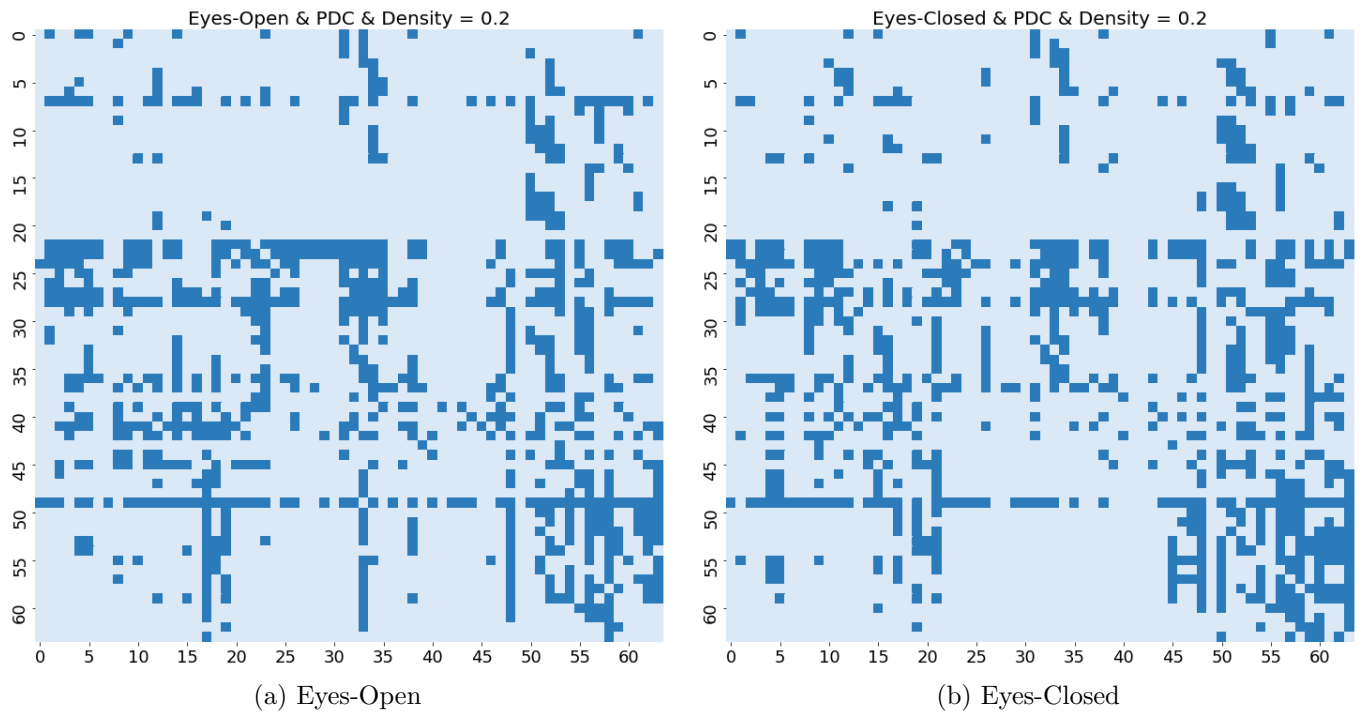


Figure 2: The binary adjacency matrices based on **PDC** estimation with **density 20%** in both resting states.

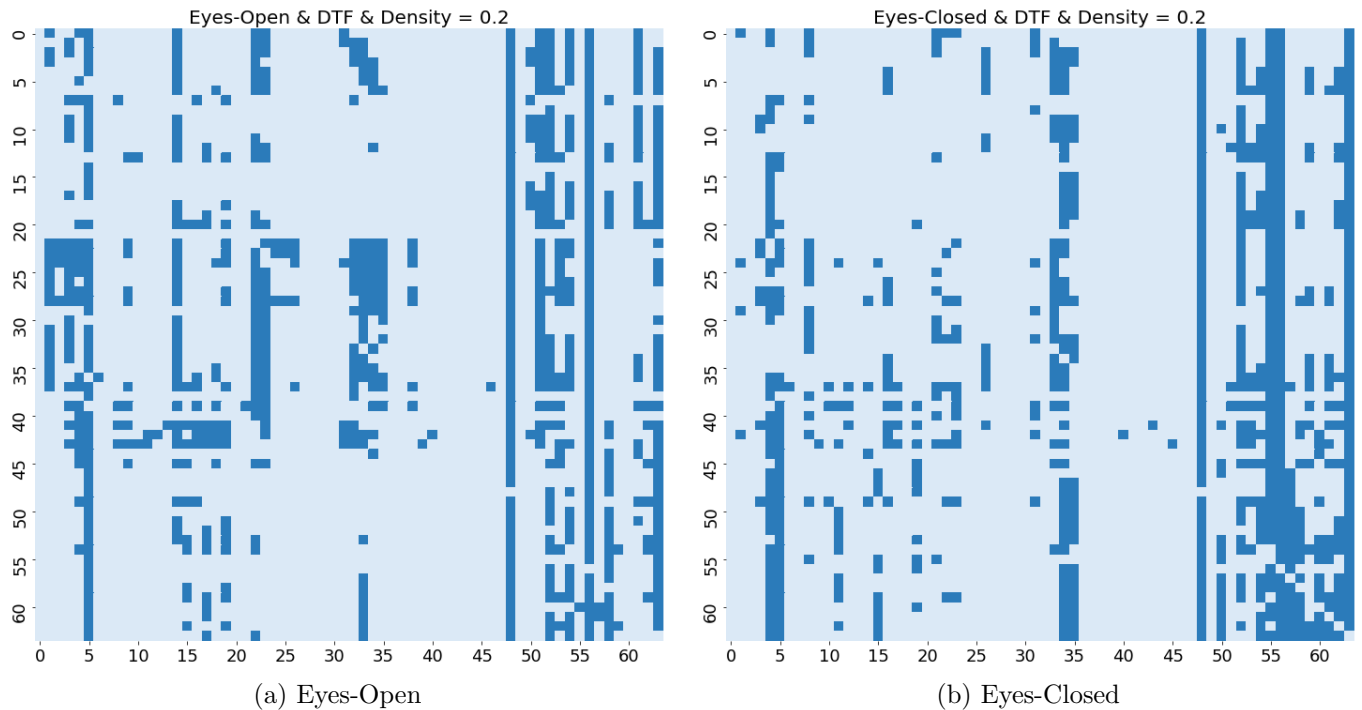


Figure 3: The binary adjacency matrices based on **DTF** estimation with **density 20%** in both resting states.

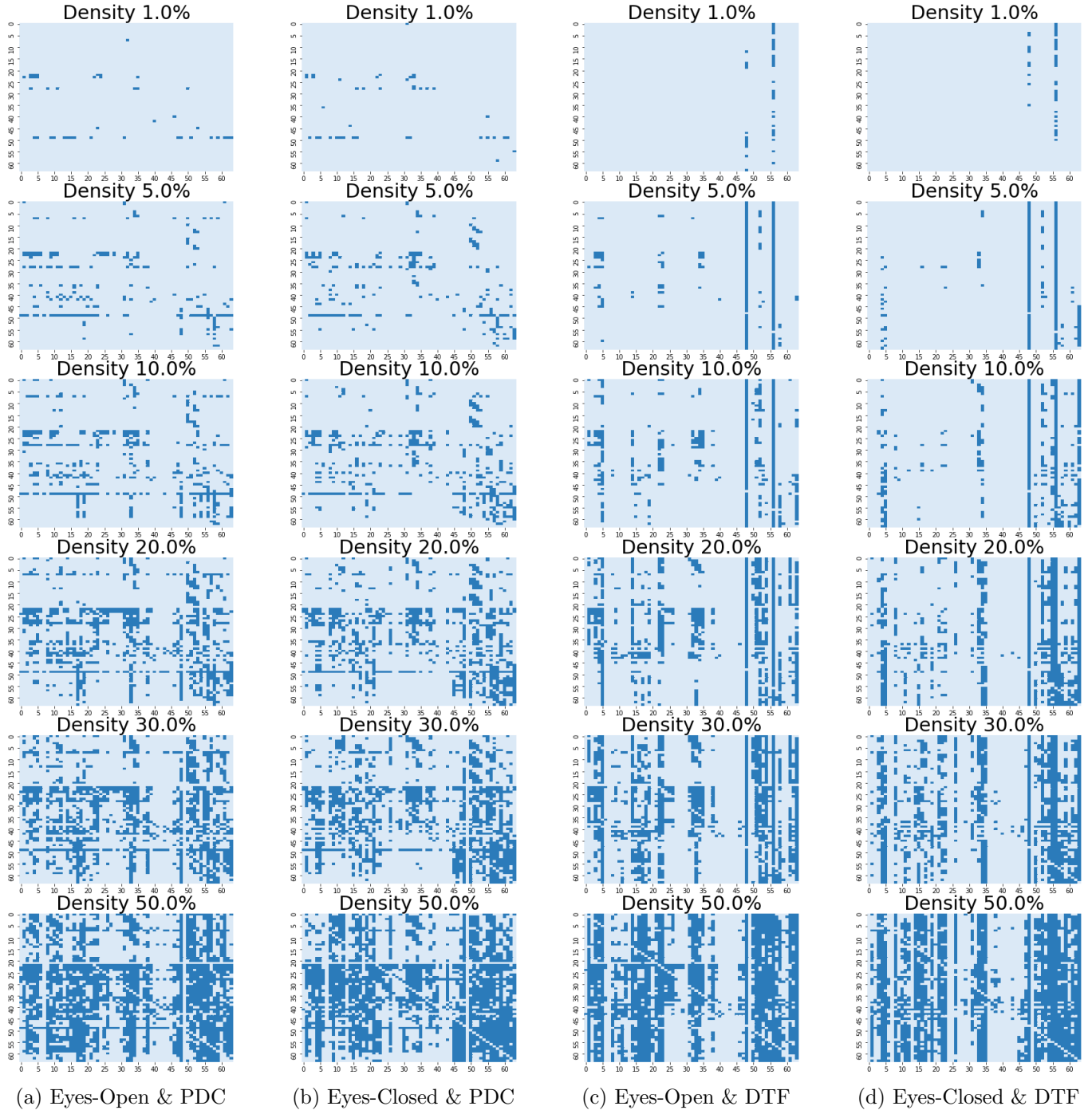
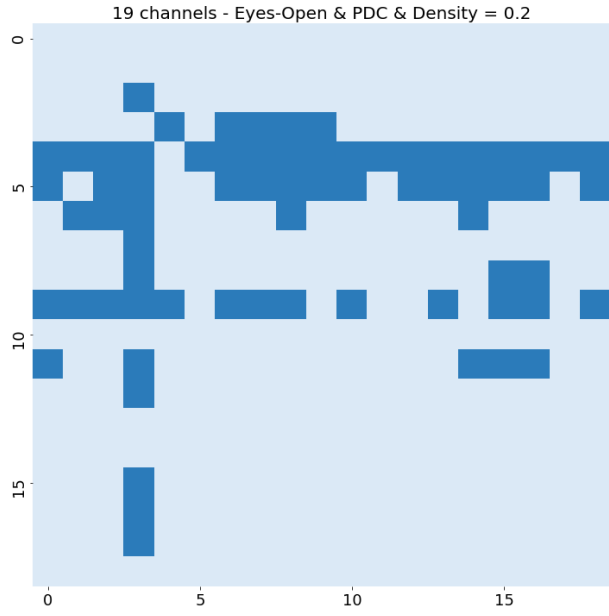
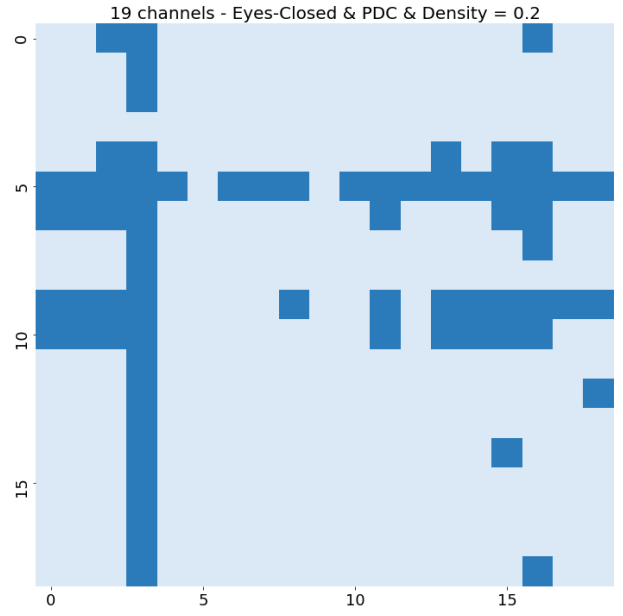


Figure 4: The binary adjacency matrices based on PDC and DTF estimations in both resting states and **Densities 1%, 5%, 10%, 20%, 30% and 50%**.

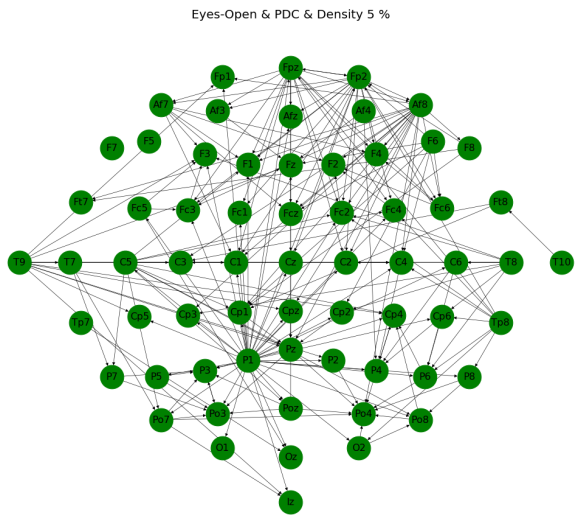


(a) Eyes-Open

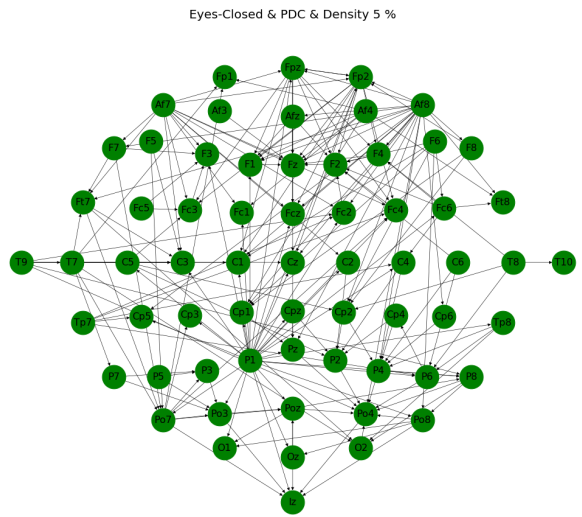


(b) Eyes-Closed

Figure 5: The binary adjacency matrices for **19 channels** based on **PDC estimation**, **significance 5%** in both resting states and **density 20%**.



(a) Eyes-Open



(b) Eyes-Closed

Figure 6: The topographical representations of **64-channels** networks based on **PDC estimation** in both resting states and **density 5%**.

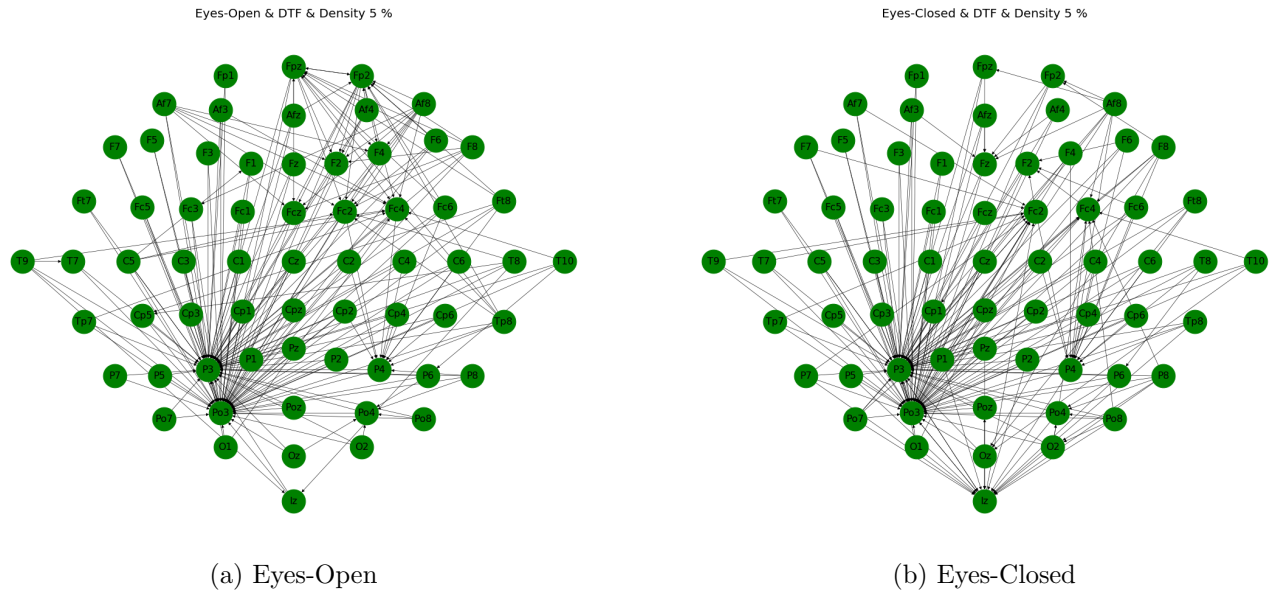


Figure 7: The topographical representations of **64-channels** networks based on **DTF** estimation in both resting states and **density 5%**.

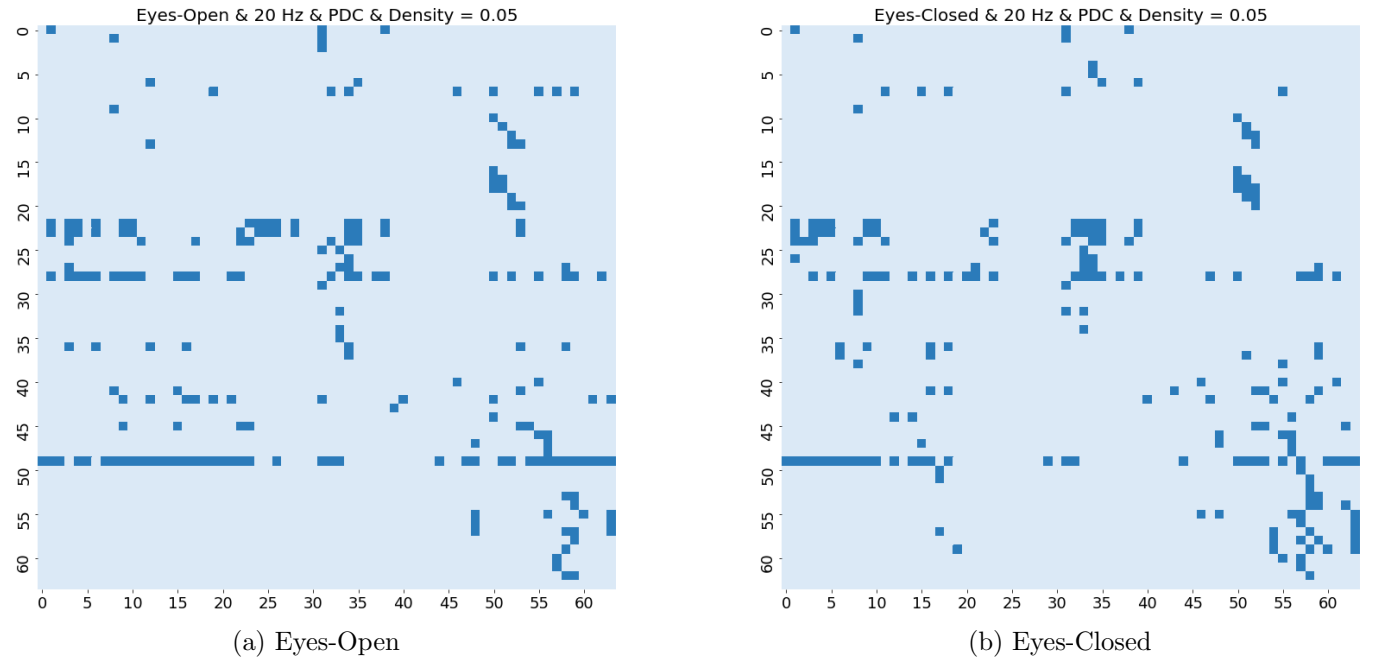


Figure 8: The binary adjacency matrices based on **PDC** estimation, frequency **20 Hz** in both resting states and **densities 20%**.

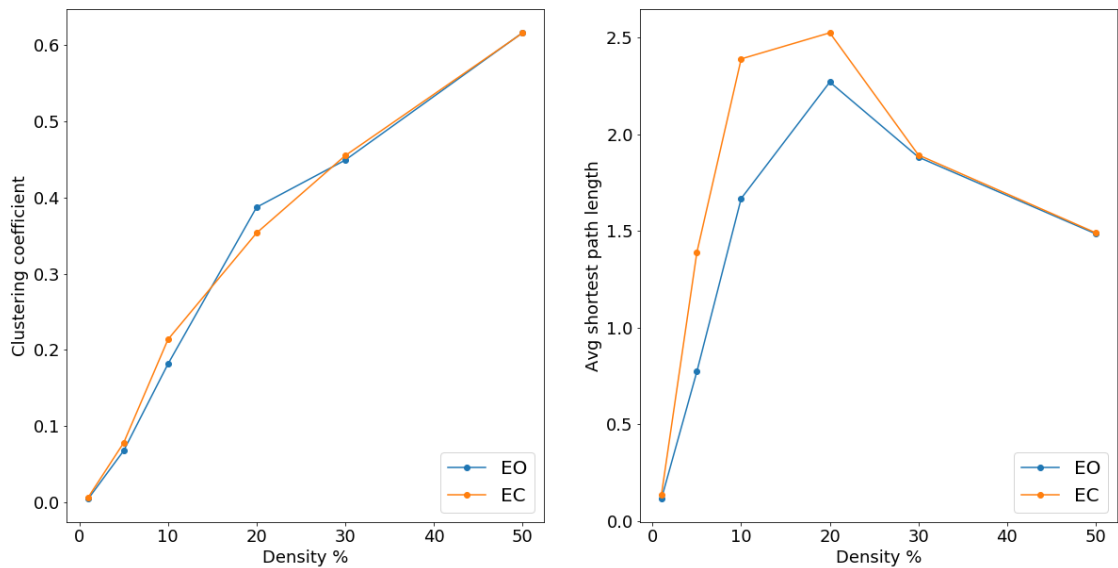


Figure 9: Global indices of the brain network at different densities

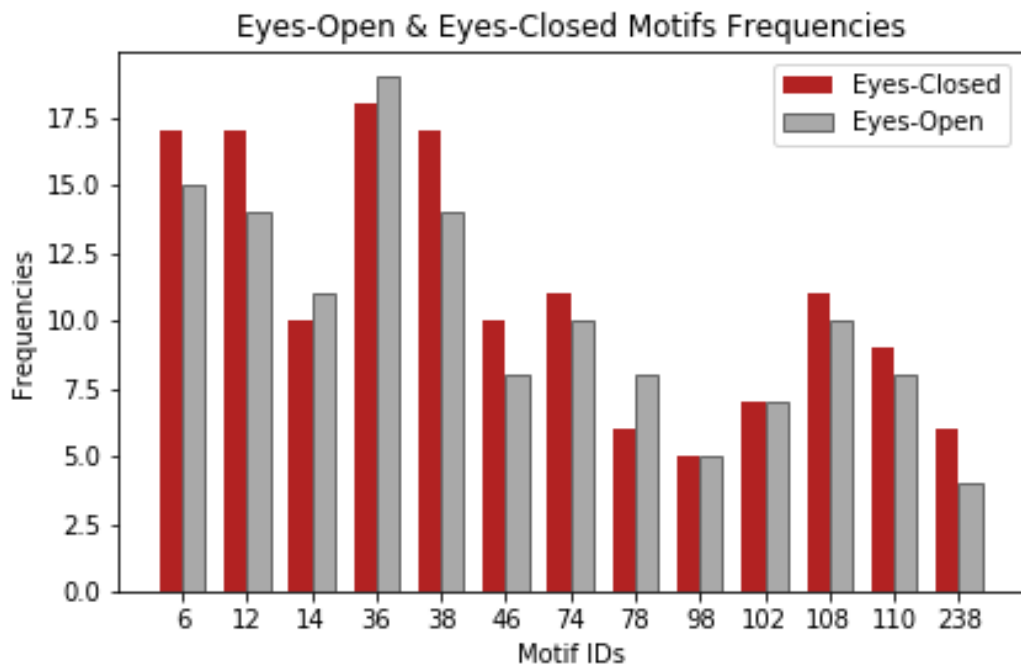


Figure 10: Histogram of motif frequencies for both rest states.

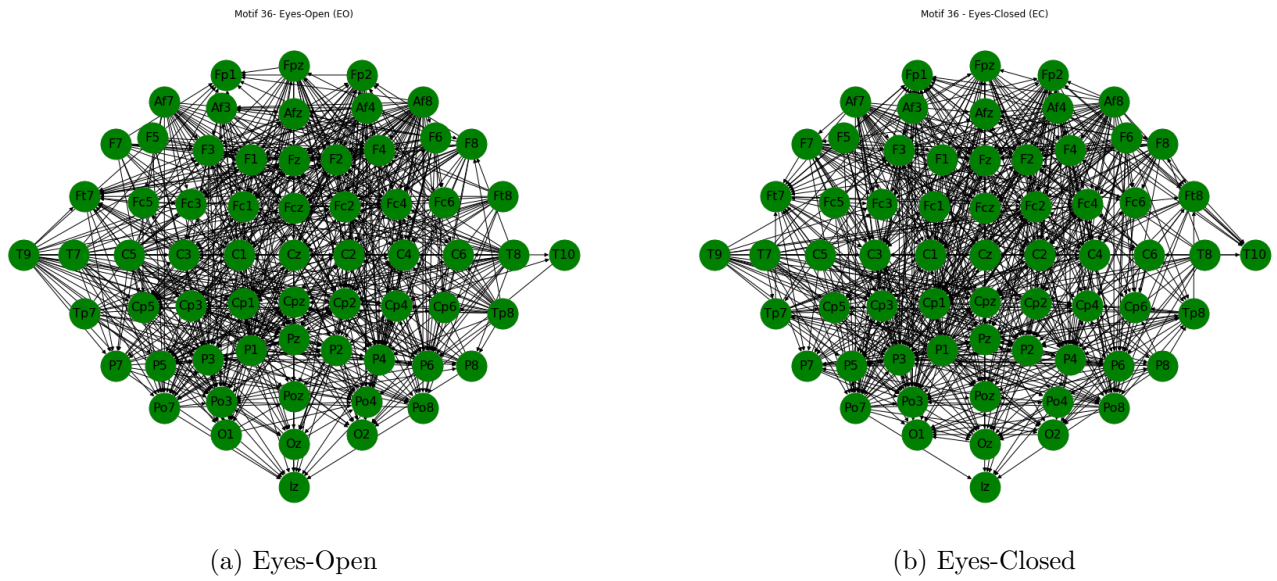


Figure 11: All edges involved to motif 36 in both resting states.

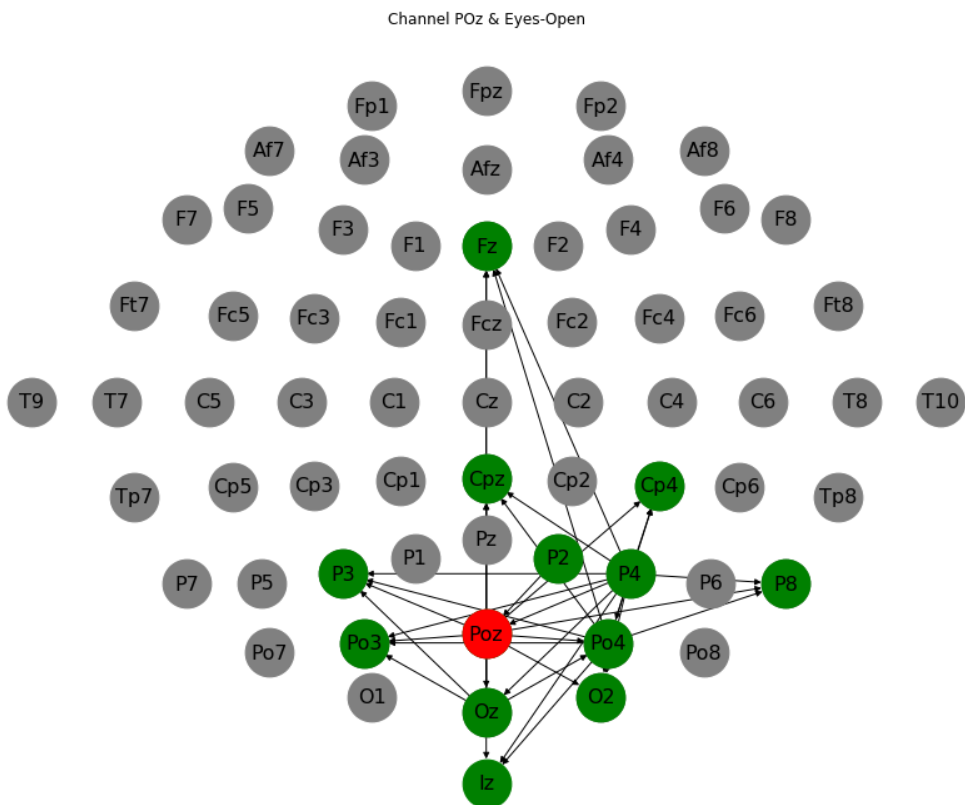


Figure 12: All edges of motifs to which the channel POz (57) was involved in Eyes-Open state.

Channel POz & Eyes-Closed

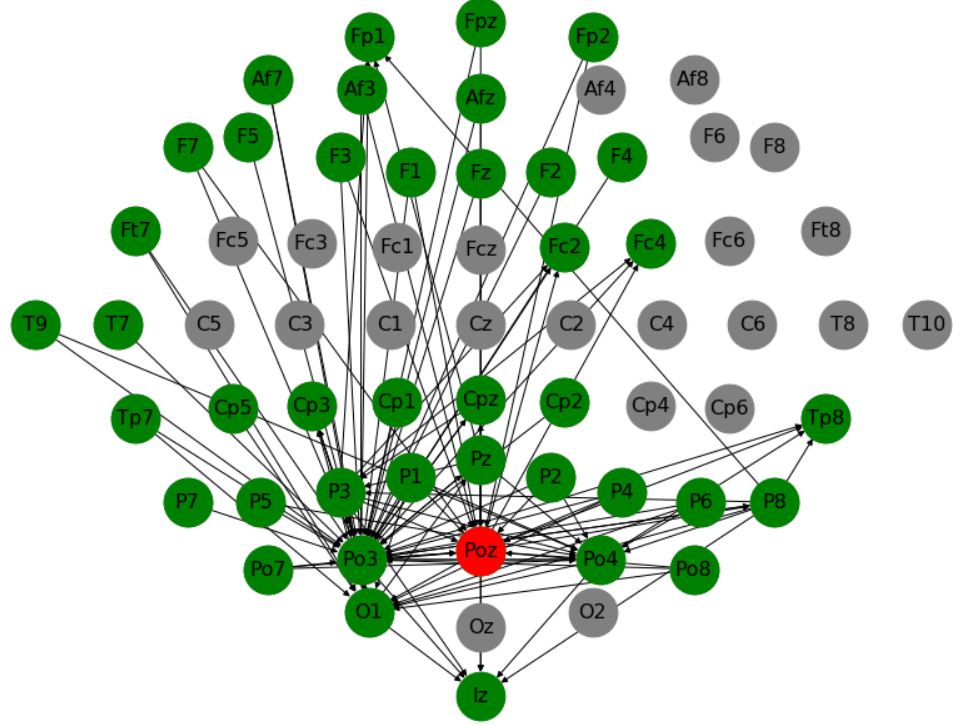
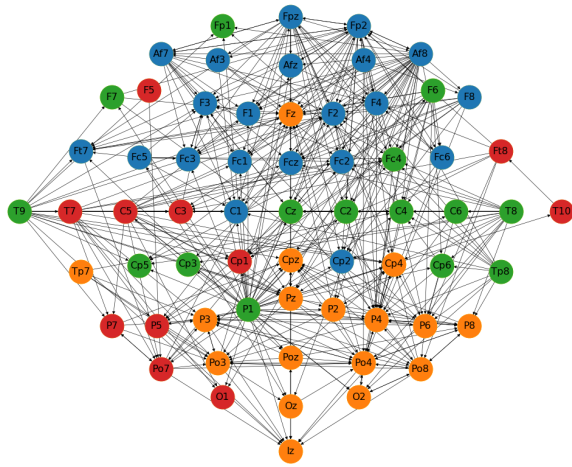


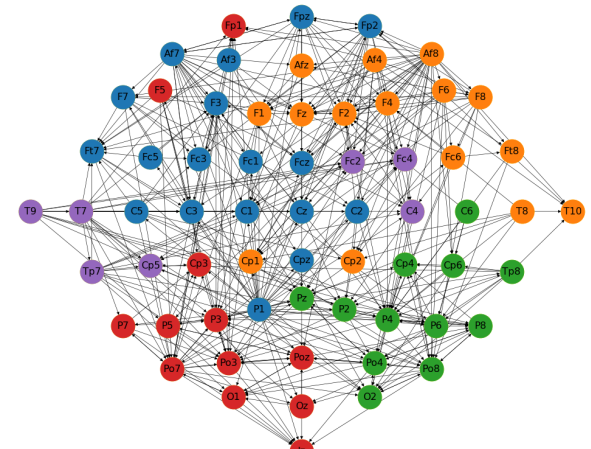
Figure 13: All edges of motifs to which the channel POz (57) was involved in Eyes-Closed.

Eyes-Open & PDC & Density=10



(a) Eyes-Open

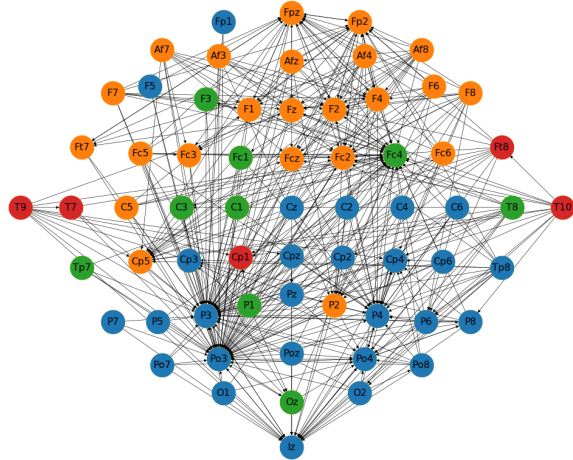
Eyes-Closed & PDC & Density=10



(b) Eyes-Closed

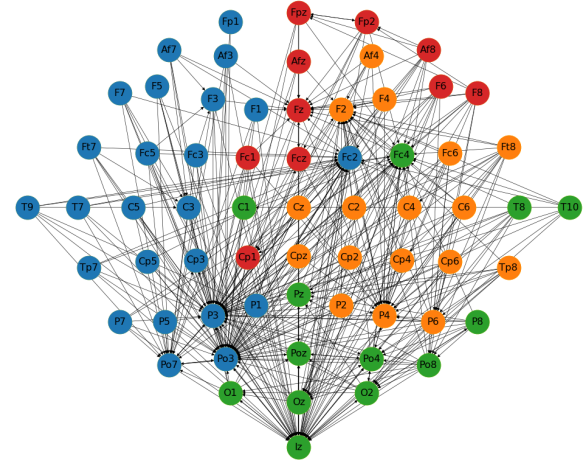
Figure 14: A graphical representation of the community structures detected by **Louvain** algorithm in network based on **PDC** and **density 10%** in both rest conditions.

Eyes-Open &amp; DTF &amp; Density=10



(a) Eyes-Open

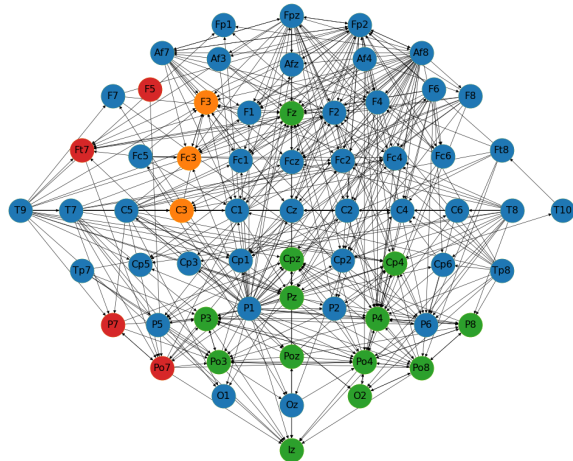
Eyes-Closed &amp; DTF &amp; Density=10



(b) Eyes-Closed

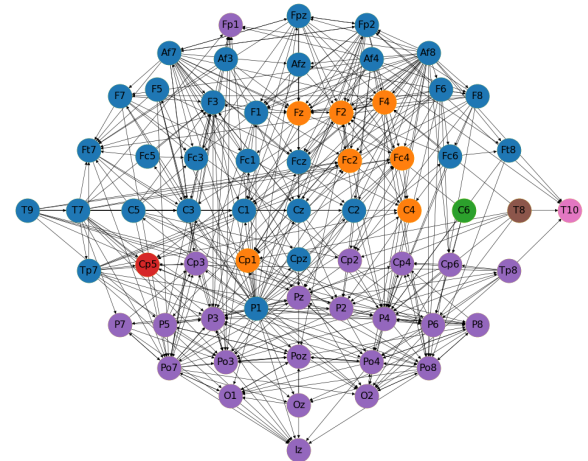
Figure 15: A graphical representation of the community structures detected by **Louvain** algorithm in network based on **DTF** and **density 10%** in both rest conditions.

Eyes-Open &amp; PDC &amp; Density=10



(a) Eyes-Open

Eyes-Closed &amp; PDC &amp; Density=10



(b) Eyes-Closed

Figure 16: A graphical representation of the community structures detected by **Infomap** algorithm in network based on **PDC** and **density 10%** in both rest conditions.

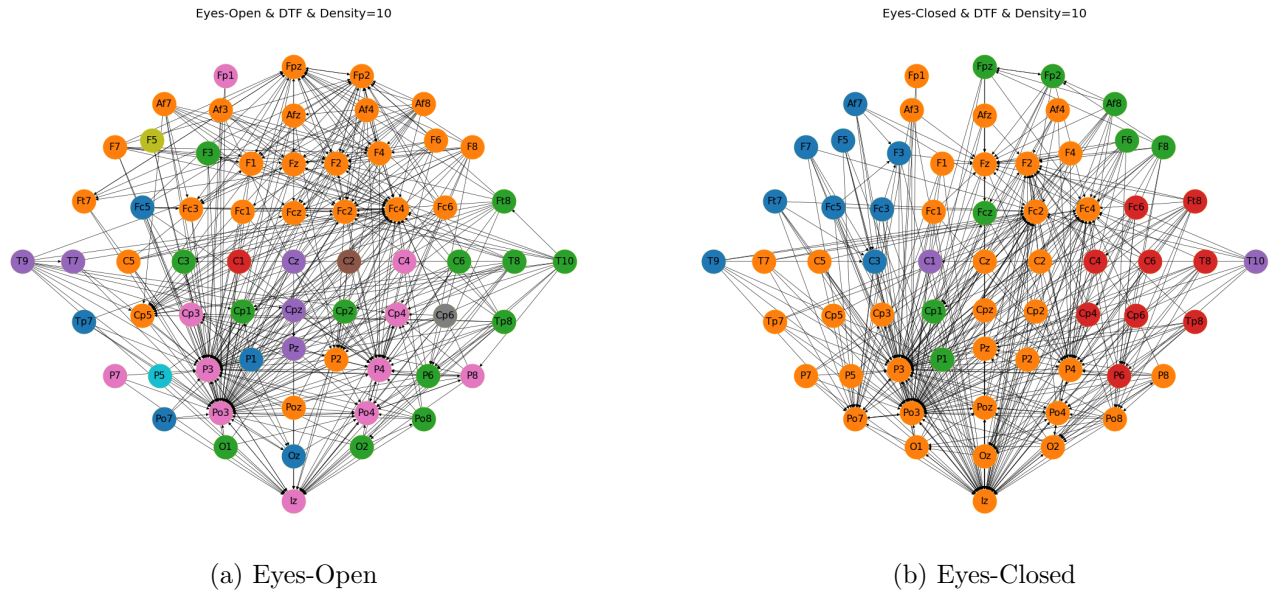


Figure 17: A graphical representation of the community structures detected by **Infomap** algorithm in network based on **DTF** and **density 10%** in both rest conditions.

## References

- [1] <https://physionet.org/physiobank/database/eegmmidb/>
  - [2] <https://github.com/holgern/pyedflib/blob/master/demo/readEDFFFile.py>
  - [3] Sporns, Olaf (2007). "Brain connectivity". Scholarpedia. 2 (10): 4695. doi:10.4249/scholarpedia.4695
  - [4] [https://en.wikipedia.org/wiki/Brain\\_connectivity\\_estimators](https://en.wikipedia.org/wiki/Brain_connectivity_estimators)
  - [5] Blinowska, Katarzyna J. "Review of the methods of determination of directed connectivity from multichannel data." Medical & biological engineering & computing vol. 49,5 (2011): 521-9. doi:10.1007/s11517-011-0739-x
  - [6] Buzsáki, György (2006). Rhythms of the Brain. New York: Oxford University Press. p. 4.
  - [7] <https://connectivipy.readthedocs.io/en/latest/>
  - [8] <https://www.weizmann.ac.il/mcb/UriAlon/download/network-motif-software>
  - [9] [https://en.wikipedia.org/wiki/Small-world\\_network](https://en.wikipedia.org/wiki/Small-world_network)
  - [10] <https://journals.plos.org/plosone/article?id=10.1371/journal.pone.0002051>
  - [11] R. Milo, S. Shen-Orr, S. Itzkovitz, N. Kashtan, D. Chklovskii, U. Alon (2002). "Network Motifs: Simple Building Blocks of Complex Networks". doi:10.1126/science.298.5594.824
  - [12] Fortunato, Santo & Hric, Darko. (2016). Community detection in networks: A user guide. Physics Reports. 659. 10.1016/j.physrep.2016.09.002.
  - [13] M. E. J. Newman, Modularity and community structure in networks, Proceedings of the National Academy of Sciences Jun 2006, 103 (23) 8577-8582; DOI: 10.1073/pnas.0601602103
  - [14] Zhao, Zhongying & Zheng, Shaoqiang & Li, Chao & Sun, Jinqing & Chang, Liang & Chiclana, Francisco. (2018). A comparative study on community detection methods in complex networks. Journal of Intelligent & Fuzzy Systems. 35. 110. 10.3233/JIFS17682.

- [15] Blondel, Vincent D; Guillaume, Jean-Loup; Lambiotte, Renaud; Lefebvre, Etienne (9 October 2008). "Fast unfolding of communities in large networks". *Journal of Statistical Mechanics: Theory and Experiment*. 2008 (10): P10008. arXiv:0803.0476. Bibcode:2008JSMTE..10..008B. doi:10.1088/1742-5468/2008/10/P10008.
- [16] M. Rosvall and D. Axelsson and C.T. Bergstrom, The map equation, *Eur. Phys. J. Special Topics* 178, 13-23 (2009) EDP Sciences, Springer-Verlag 2010 DOI: 10.1140/epjst/e2010-01179-1